


# Three-dimensional rotational angiography in congenital heart disease: Present status and evolving future

Sok-Leng Kang MBBS, MRCPCH, MSc<sup>1</sup>  | Aimee Armstrong MD, FACC, FSCAI<sup>2</sup> |  
Gregor Krings MD, PHD<sup>3</sup> | Lee Benson MD, FRCPC, FACC, FSCAI<sup>1</sup> 

<sup>1</sup>Division of Cardiology, The Labatt Family Heart Center, The Hospital for Sick Children, The University of Toronto School of Medicine, Toronto, Canada

<sup>2</sup>The Heart Center, Nationwide Children's Hospital, The Ohio State University College of Medicine, Columbus, Ohio

<sup>3</sup>Children's Heart Center, Utrecht University, Utrecht, Netherlands

## Correspondence

Lee Benson, The Hospital for Sick Children, 555 University Ave, Toronto, Ontario, Canada, M5G 1X8.  
Email: lee.benson@sickkids.ca

## Funding information

Sok-Leng Kang has no disclosures. Aimee Armstrong and Lee Benson have received no funding for this publication and research granted from Siemens Medical Solutions USA, Inc. Gregor Krings has received no funding for this publication and he is a member of Siemens Healthineers Advisory Board.

## Abstract

Three-dimensional rotational angiography (3D-RA) enables volumetric imaging through rotation of the C-arm of an angiographic system and real-time 3D reconstruction during cardiac catheterization procedures. In the field of congenital heart disease (CHD), 3D-RA has gained considerable traction, owing to its capability for enhanced visualization of spatial relationships in complex cardiac morphologies and real time image guidance in an intricate interventional environment. This review provides an overview of the current applications, strengths, and limitations of 3D-RA acquisition in the management of CHD and potential future directions. In addition, issues of dosimetry, radiation exposure, and optimization strategies will be reviewed. Further implementation of 3D-RA will be driven by patient benefits relative to existing 3D imaging capabilities and fusion techniques balanced against radiation exposure.

## KEYWORDS

angiography, cardiac catheterization, congenital heart defects, rotational, three-dimensional imaging

## 1 | INTRODUCTION

The clinical implementation of three-dimensional (3D) imaging represented a significant advancement in the diagnosis and treatment of congenital heart lesions by providing visualization of anatomical spatial relationships, enhancing understanding of complex structural relationships seen in congenital heart lesions. As such, it has proven effective within the continuum from pre-surgical planning to procedural integration.<sup>1-4</sup> In this context, 3D rotational angiography (RA) is an emerging imaging technology acquired during cardiac catheterization that permits rapid acquisition of high resolution volumetric datasets through rotation of a C-arm mounted flat panel detector, in a manner similar to computed tomography (CT).<sup>5-10</sup> The terms angiographic CT and flat detector or cone beam CT are used interchangeably in the literature. This article provides an overview of the role and utility of 3D-RA in the assessment and management of congenital heart disease (CHD), highlighting its strengths and

limitations, and discusses future perspectives, including comments on radiation exposure, the difficulties with dosimetry and specific dose-reduction strategies.

## 2 | THE EMERGENCE OF 3D-RA

In 1964, Lucien Campeau and Jacques Saltiel (Montreal, Canada) were the first to publish angiograms of congenital heart lesions with the patient fixed in a cradle and rotated 90° within a C-arm.<sup>11</sup> Between 1965 and 1973, Schad and Brunner (Stuttgart, Germany) used a 180 degree rotation of the cradle with an ECG-triggered self-developed power injector to perform rotational angiograms in patients with CHD.<sup>12</sup> In 1972, Cornelis and colleagues described the technique of rotating the X-ray tube around the patient during cerebral angiography, with clinical adoption for neurosurgical procedures reported a decade later.<sup>13,14</sup> Further refinements in the rotational

technique and concurrent development of 3D volume rendering software culminated in the first 3D reconstruction of RA sequences in 1997, opening the way for expansion in clinical applications from neurosurgical applications to real time evaluation of spinal interventions, abdominal aortic aneurysm repair, and hepatic vascular chemembolization.<sup>15-20</sup> As an emerging technology, it was first exploited in the cardiovascular system for coronary evaluation in 1998,<sup>21,22</sup> with gradual integration into electrophysiology procedures and management of CHD reported in the mid-2000's.<sup>23,24</sup> Primary enabling technologies for widespread clinical implementation were the introduction of digital flat panel detectors capable of ultra-high spatial resolution with large volume coverage and the rapid increase in computational speed for timely 3D image reconstruction.<sup>25</sup> Today, 3D-RA is widely used for assessment, monitoring, and guidance in various interventional, surgical, and therapeutic applications.

### 3 | OVERVIEW OF TECHNIQUE

#### 3.1 | Image acquisition

Image acquisition, which is done in only single plane at this time, begins with isocenter positioning of the region of interest (ROI) to ensure that it is fully incorporated in the field of view during the rotation. The ROI is centered on the frontal flat panel, after which the gantry is rotated 90° and the table height adjusted. Acquisition time, and rotation arc (>180°) determine the speed (up to 55°), which varies depending on the hardware installation. Adjustment of frame rate can be made by the vendor when setting the dose programs. During detector rotation, contrast is administered with a power injector(s) (or in combination with hand injections, for multiple injection sites) at a contrast dose ranging from 0.5 to 2 cc/kg, usually diluted with normal saline (50%-66% contrast).<sup>5,8,26,27</sup>

For optimal image quality, the ROI must remain opacified throughout acquisition. To achieve this, several techniques can be employed, including rapid ventricular pacing, injection into the cardiac chamber proximal to the ROI, and temporary balloon occlusion of the run-off vessel or the pulmonary artery (PA) in high-flow lesions. Programming a time delay for image acquisition after contrast injection begins also allows better ROI opacification (eg, 0.5-2s for PA and aorta, 1-3s for cavopulmonary connections and 5-6s for pulmonary veins). In complex hemodynamic situations, such as valvar regurgitation, high shunt flows or arrhythmias, a test bolus of contrast with fluoroscopic monitoring has been reported to help determine the optimal scan delay time.<sup>7,9,27</sup> Rapid ventricular pacing (to decrease the systolic blood pressure by ~50%) or bolus injection of adenosine (0.1 to 0.4 mg/kg) have also been used to decrease cardiac output transiently, delaying washout of contrast media. The decrease in cardiac output also reduces metallic artifact and improves assessment of distal pulmonary arteries by limiting the opacification of the pulmonary veins and of coronary artery fistulae and aneurysms by reducing cardiac motion.<sup>9</sup> While modification of the cardiac output is not needed in imaging a cavopulmonary connection due to the lack of pulsatility, simultaneous injections into two

identical (same length and French size) catheters positioned in different portions of the cavopulmonary connection (eg, superior and inferior vena cava in a total cavopulmonary connection), connected back to a single injector, enables the entire PA connection to be imaged with a single acquisition.<sup>27</sup> This technique is also useful in the case of bilateral bidirectional cavopulmonary connections, avoiding negative contrast wash out in one of the branch PAs, from unopacified contralateral superior caval flow. Suspension of breathing or ventilation is essential to avoid respiratory motion artifact. Finally, having the interventional wire in place during the injection allows for optimal overlay of the 3D image on live fluoroscopy during the subsequent intervention, as the wire often distorts the anatomy.

#### 3.2 | Image analysis and 3D reconstruction

The acquired 2D rotational angiogram is available for immediate review, and the automatic 3D reconstruction on the workstation requires <1 minute to display. The most widely used reconstruction algorithm is the Feldkamp, Davis and Kress weighted filtered back projection algorithm because of simplicity of implementation and computational efficiency.<sup>28</sup> However, due to the iteration required for calculating this algorithm, artifacts may be observed in the reconstruction for 3D-RA with a short scan angular range. In addition, artifacts inherent to the measurement or reconstruction process, such as noise, scatter, beam hardening, and ring and shading artifacts, may interfere with diagnostic interpretation. Knowledge of the presence of such artifacts and their appearance is necessary.<sup>29</sup>

The ROI can be isolated with a wide range of manual and automated segmentation techniques. The most popular segmentation methods fall into two categories: (a) image-driven approaches, including threshold-based, edge-based, and region-growing segmentation and (b) model-driven approaches based on prior models. Model-based segmentation relies on mathematical representation of the expected geometry of the structure of interest registered into large training datasets.<sup>30</sup> A combination of segmentation approaches can be used, and the criterion for the choice of technique is the segmentation accuracy. The 3D volume is presented using several visualization techniques. Multiplanar reformation (MPR) displays 2D image slices simultaneously from several orientations, allowing the user to scroll through the reconstructed volume one slice at a time (down to <0.5 mm), to delineate morphological details or to make measurements, which do not require manual calibration. Measurements should not be obtained from the 3D reconstruction, as it is much more susceptible to window-leveling than is the MPR. Maximum intensity projection (MIP) displays the voxel with the highest attenuation value in the visualization planes or slabs with increased thickness, best suited for depicting small vascular structures.<sup>31</sup> Three-dimensional endoscopic fly-through techniques provide unique intraluminal view of blood vessels, valuable for assessing endovascular stents, aortic aneurysms, vessel wall irregularities, and calcification.<sup>32</sup> The 3D reconstruction can be rotated in any angle to view the ROI in detail and allows the interventionist to find the optimal gantry angles for subsequent 2D angiography.

### 3.3 | Multimodal image fusion

The 3D reconstructions from RA, CT, and magnetic resonance imaging (MRI) can be superimposed over live fluoroscopy to produce 3D roadmaps.<sup>10,26</sup> Images are automatically registered to or in geometric correspondence with the C-arm coordinates, allowing the system to track the spatial relationships of all points within the X-ray field, including table position. CT or MRI road mapping, however, requires appropriate registration of a segmented pre-procedure volume with the X-ray system and can be limited by lack of visible bones for registration and by differences in arm position, respiration, and even growth of the patient between the CT or MRI and the catheterization. A variety of registration modalities are currently in use, including fiducial registration to 2D visual matching.<sup>10,32-37</sup>

## 4 | THE ROLE AND UTILITY OF 3D-RA IN CHD

Children with complex congenital heart lesions present an imaging challenge due to the complexity and variability of structural relationships. Conventional 2D angiography is limited by vessel overlap and foreshortening in addition to lack of depth information. These limitations do not exist in the 3D representation of cardiac structures, and, therefore, multimodality 3D imaging and 3D image fusion are emerging as critical imaging adjuncts in the congenital cardiac catheterization laboratory.

The introduction of 3D-RA has allowed the development of a management paradigm offering a "one-stop" 3D imaging solution for pre-therapeutic assessment, treatment guidance, and posttreatment evaluation. Three-dimensional RA provides rapid image acquisition at high spatial resolution (z-axis resolution of 0.2 mm compared to 0.5 mm for multidetector-CT (MDCT) and 1.5-2 mm for MRI angiography), with less contrast and radiation dose than MDCT reported for certain applications.<sup>38-40</sup> Since the first articles describing the use of 3D-RA for CHD in 2010, numerous publications have emerged supporting its feasibility and clinical utility.<sup>5,7,9,27,41-48</sup> Several studies have reported a high frequency (71% to 98%) of diagnostic quality images in a variety of CHD lesions and, importantly, an additive yield compared to standard 2D biplane angiography.<sup>5,42,45,49</sup> Variability of image quality may in part relate to learning curves associated with image acquisition in the early studies. With regard to quantitative assessment, excellent correlation ( $r = 0.94$  to  $0.99$ ) of measurements between aortic and PA dimensions on 3D-RA and 2D angiography have also been demonstrated in multiple studies.<sup>42-44,50</sup> Potential benefits of overlay on live fluoroscopy include improved procedural efficacy and safety, shorter fluoroscopy times, and reduced overall radiation dose and contrast administration.<sup>8,10,44-46,51</sup> From a safety perspective, adverse events from 3D-RA have not been reported in the literature.

### 4.1 | Limitations

A significant limitation of current RA technology is the inability to gate during the cardiac cycle, as the reconstructed images are signal

averaged. As in MRI angiography, the temporal information obtained by 2D angiography is lost in RA, and motion artifacts result in degradation of the quality of the reconstruction. There is thus the potential for inaccuracy in the measurements from the reconstructed image. Rapid ventricular pacing also leads to a decrease in the size of vessels masking the true dimensions of these dynamic structures. This typically leads to undersized aortic dimensions when stenting vessel lesions such as CoA or the aortic arch. In main and branch PA interventions, 3D-RA associated under-sizing often is non-relevant.<sup>42</sup> The issue of respiratory motion is avoided with suspension of ventilation. Recently, there has been progress in motion compensation algorithms to optimize the reconstruction process and model accuracy from RA data.<sup>52-56</sup> However, in case of an anatomic shift (patient movement, anatomy shift by sheath/wires, etc.), manual correction of the 3D overlay in relation with the live fluoroscopy is simple by giving a short contrast injection to re-register.

## 5 | CLINICAL APPLICATIONS IN CHD

### 5.1 | Evaluation of right-sided obstructive lesions

Obstructive lesions in the right heart may occur at any level from the mid-right ventricle (RV) to the peripheral PA with highly complex morphology and often with serial stenoses at multiple levels. Further, vessel overlap and foreshortening are common in 2D imaging of complex PA lesions. A single RA provides detailed anatomy from the trabeculations of the RV to the tertiary branch PAs and a volume-rendered 3D reconstruction that can be viewed in an almost infinite number of virtual angles.<sup>5,7-9,27,48</sup> The length and geometry of the surgically reconstructed RV outflow tract or RV-to-PA conduit and its relationship to the sternum can be delineated, particularly in the presence of aneurysmal formation, dilation, or angular distortion.<sup>57,58</sup> Similarly, the superior spatial resolution afforded by 3D-RA allows definition of branch/peripheral PA anatomy and the relationship of the PAs to the airways and other vessels (Figures 1 and 2).

### 5.2 | Percutaneous pulmonary valve implantation planning and guidance

Percutaneous pulmonary valve implantation (PPVI) is an established alternative to surgery for RV-to-PA conduit and bioprosthetic valve dysfunction. More recently, its application has extended to use in the native RV outflow tract, which constitutes the majority of patients with a dysfunctional RVOT.<sup>59-62</sup> Careful patient selection and detailed multimodality imaging of the relevant anatomy are essential to avoid catastrophic complications such as coronary compression, pulmonary arterial injury or rupture, and device embolization.<sup>63</sup> Here, 3D-RA offers significant advantages over conventional angiography in three main areas: 3D evaluation of RV outflow tract morphology, procedural guidance with 3D image overlay, and assessment of potential coronary and LVOT/aortic compression with RVOT balloon inflation (Figure 3). Both the 2D rotation and the 3D reconstruction can profile the coronary course and distance from the conduit during balloon assessment.

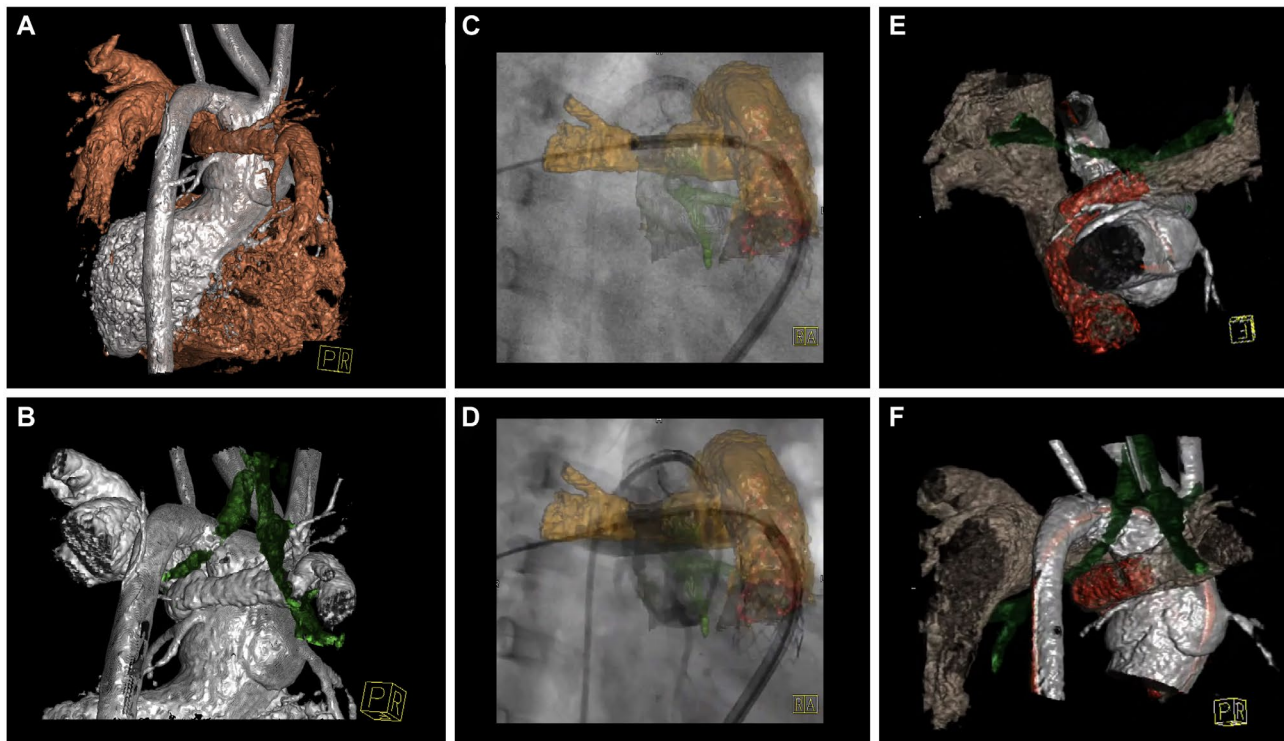


**FIGURE 1** (A) Posterior view of 3D-RA with simultaneous contrast injection in right and left ventricle, showing the LCA ostium close to the RPA stenosis and large LPA in a 3-year-old patient with hypoplastic left heart complex post neonatal Ross Konno. (B) Simultaneous airway visualization showing mild compression of left bronchus and its close relation with the stenotic RPA. (C) RPA stent implantation with 3D-RA roadmap and (D) with simultaneous LCA angiography. The LCA is shown in green. (E,F) 3D-RA after RPA stent implantation. 3D-RA, three-dimensional rotational angiography; LCA, left coronary artery; LPA, left pulmonary artery; RPA, right pulmonary artery

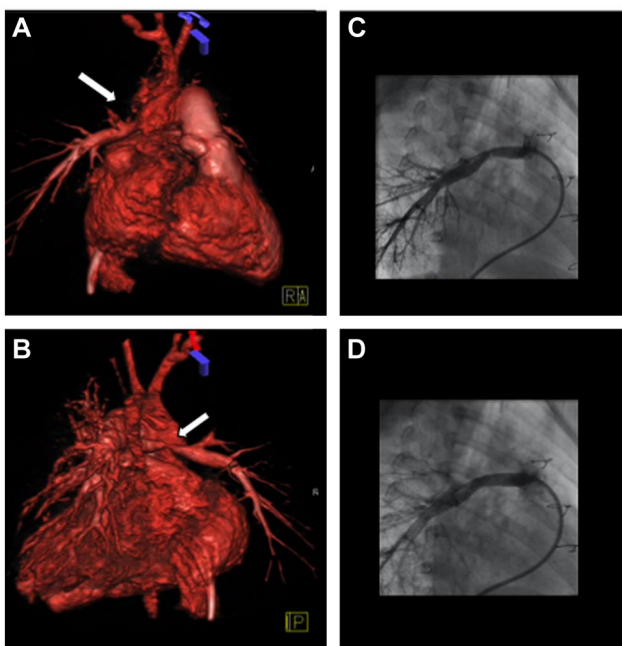


**FIGURE 2** A 2-year-old child with double outlet right ventricle after repair with an RV-to-PA conduit and proximal RPA stenosis. (A, B) Elongation of the right PA with severe stenosis related to compression by the aorta (arrow) and (C) Corresponding 2D angiogram (D) Final angiogram after balloon dilation. PA, pulmonary artery; RV, right ventricle

Furthermore, the 3D reconstruction allows assessment of the calcification patterns throughout the RVOT, a risk factor for PPVI associated conduit injury, which cannot be assessed by MRI.<sup>64</sup>

### 5.3 | Single ventricle circulation assessment

In patients with partial or total cavopulmonary connections, 3D-RA is particularly applicable due to the slow blood transit time and limited vessel pulsatility. Several reports of 3D-RA profiling of the cavopulmonary anastomosis and pulmonary arteries have shown improved identification of stenotic lesions at the anastomotic sites (compared to 2D angiography), in addition to elucidation of the underlying mechanisms.<sup>9,41,42</sup> (Figure 4). Furthermore, knowledge of the 3D relationship of the trachea and bronchi to the surrounding cardiovascular structures can help prevent compression of the airway with an intravascular stent.<sup>43</sup> Finally, adjunctive visualization techniques such as MPR and MIP can add diagnostic value.<sup>32</sup> Effective use of 3D image overlay has also been described for closure of Fontan baffle fenestrations.<sup>65</sup>

### 5.4 | Delineation of aortopulmonary collaterals and pulmonary blood supply

Tetralogy of Fallot with pulmonary atresia is often associated with major aortopulmonary collateral arteries (MAPCAs) with highly variable



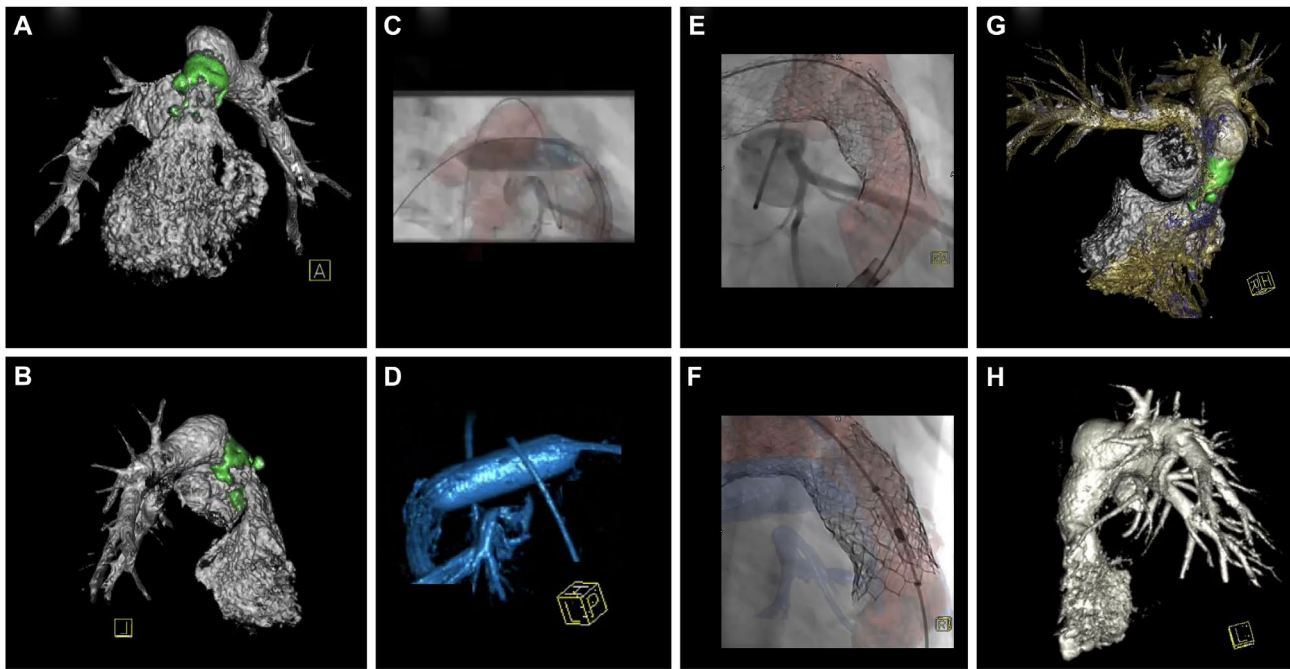


**FIGURE 3** Images of a 10-year-old child with an interrupted aortic arch, VSD, and lusoric artery after initial neonatal Ross-Konno operation and 6 years after subsequent homograft replacement. (A, B) 3D-RA fusion with a CT angiogram obtained pre-cardiac catheterization with a non-contrast 3D-RA outlining circumferential calcification of the homograft in relation with aorta and coronary arteries. (C) Balloon interrogation in the RPA with a simultaneous LCA angiogram. (D) 3D-RA reconstruction demonstrating uncompressed LCA. (E) LCA angiography after implantation of two stents from the MPA into RPA. (F) Post PPVI. (G, H) Overlay of pre-catheterization CTA (silver with green calcification) and 3D-RA after PPVI (gold) in a cranial angulated frontal view (G) and LAO projection (H). LCA, left coronary artery; PPVI, percutaneous pulmonary valve implant; RPA, right pulmonary artery

morphology. In many centers, invasive angiography remains the primary assessment tool due to surgical preference or inadequate spatial resolution with MRI.<sup>66</sup> With biplane projections, the often-tortuous course of the MAPCAs is difficult to profile in its entirety. In contrast, 3D-RA provides superior depiction of the MAPCAs from their origin to each pulmonary segment with a single injection in the aorta.<sup>5,27,44</sup> The high-fidelity 3D reconstructed roadmap of the MAPCAs, including its relationship to the trachea and esophagus, facilitates surgical planning.

### 5.5 | Airway assessment

Airway anomalies are not uncommon in the presence of complex cardiovascular malformations. Accurate definition of airway compromise and its etiology has significant implications for surgical and interventional planning and post-procedural recovery.<sup>43,47</sup> In children requiring cardiac catheterization, 3D-RA allows assessment of the topological relationships of the vascular structures and the airway and their potential interaction (Figure 1).<sup>47</sup> Recently, a novel oval stent technique was described to treat left PA stenosis, while preventing compression of the left bronchus, using 3D-RA to delineate the vessel-airway relationship.<sup>67</sup> Even though MDCT has been used traditionally to assess the airway, the median radiation exposure during 3D-RA has been reported to be well below the effective dose of pediatric chest MDCT, using a conventional or low dose protocol, while achieving similar spatial resolution.<sup>39</sup>

### 5.6 | Aortic intervention planning and guidance

In patients with coarctation of aorta, many anatomic characteristics, such as tortuosity, arch hypoplasia, aneurysm, or multiple levels of obstruction, can be difficult to appreciate with conventional angiography (Figures 5 and 6). While CT or MRI is often used for pre-procedural planning, 3D-RA performed during the catheterization has been shown to impact positively on the performance and outcomes of the procedures.<sup>8,44,45,68</sup> Starmans et al reported a higher success rate for both arch angioplasty and stenting of coarctation with 3D-RA, attributed to superior imaging and hence improved or more aggressive treatment.<sup>45</sup> Another study reported significantly reduced fluoroscopy time and radiation dose when 3D-RA was used compared to conventional angiography.<sup>8,44</sup>

### 5.7 | Patent arterial duct interventions

Indications for intervention on the patent arterial duct are to maintain patency in those with duct-dependent congenital cardiac lesions and to occlude it in children with symptomatic or hemodynamically significant left to right shunts. Three-dimensional RA has been described in both situations to improve anatomical assessment and guide intervention.<sup>5,27,49,69-71</sup> In the setting of hybrid hypoplastic left heart syndrome palliation, it has been used to aid visualization of ductal morphology and adjacent vessels for stent selection and placement.<sup>69</sup> Almost half of newborns with a

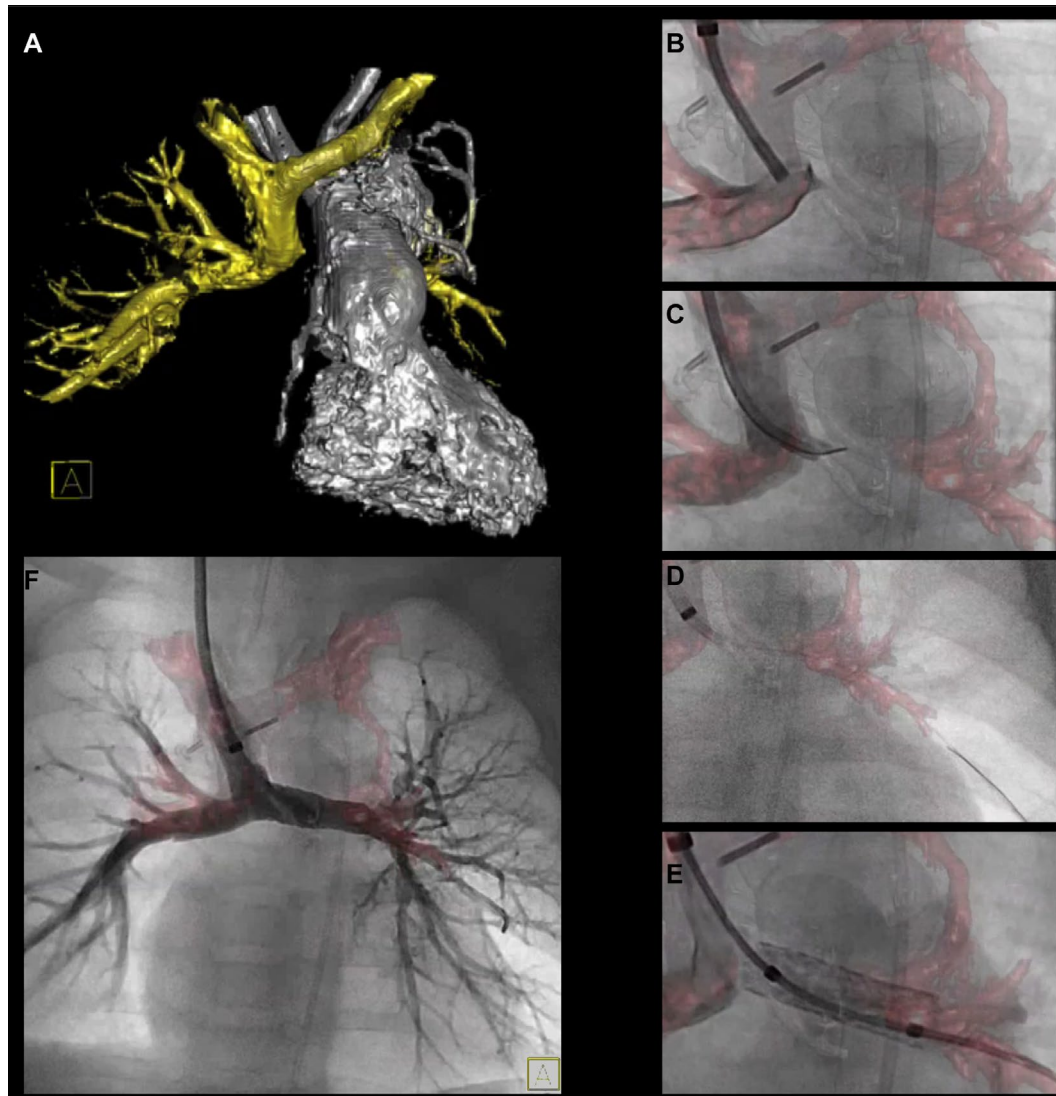


**FIGURE 4** Images of a 6-month-old child with a bidirectional cavopulmonary anastomosis and complete LPA occlusion. (A) Initial 3D-RA with simultaneous contrast injection in both jugular veins and systemic ventricle with rapid pacing shows an occluded LPA perfused by small a collateral artery. (B-D) Re-canalization of LPA with co-axial coronary wires, micro catheter, multipurpose guide catheter, and finally a long sheath. (E) Successful LPA stenting, and (F) final angiogram. LPA, left pulmonary artery

ductal-dependent pulmonary circulation referred for ductal stenting have a tortuous duct. Three-dimensional RA has the ability to image the duct from a wide range of viewing angles with one acquisition. Further, the depiction of ductal origin and point of insertion onto the proximal pulmonary arteries can identify subtle stenosis, which can influence treatment decisions and guide the procedure.<sup>27</sup> In the context of PDA closure, several authors have reported the usefulness of 3D-RA in delineating ductal orientation and morphology for selection of implantable devices.<sup>70,71</sup>

## 5.8 | Coronary artery assessment

Rotational angiography for evaluation of the coronary system was the earliest application of this technology in the cardiovascular system. Through innovative adaptations, the technique has progressed from manual C-arm rotation to dual axis rotational angiography

(DARCA).<sup>21,72</sup> Rather than a simple arc, dual axis rotational acquisitions are programmed to move the C-arm gantry simultaneously in both the RAO-LAO and cranial-caudal axes, specifically designed to reduce the effect of vessel foreshortening. In addition to improved coronary visualization and assessment, coronary RA has been demonstrated to decrease contrast dose, radiation exposure and overall procedure time, with a safety profile comparable to standard coronary angiography in adult studies.<sup>73-76</sup> Given the advantages of coronary artery visualization in 3D, application of RA has been extended to complex pediatric coronary lesions such as pulmonary atresia with intact ventricular septum, Kawasaki disease, aorto-ventricular and coronary artery fistulae, and other congenital coronary anomalies.<sup>9,24,38</sup> More recently, the feasibility and safety of DARCA have been reported for the evaluation of graft coronary vasculopathy in pediatric heart transplant recipients with no increase in radiation exposure or contrast use.<sup>77,78</sup>

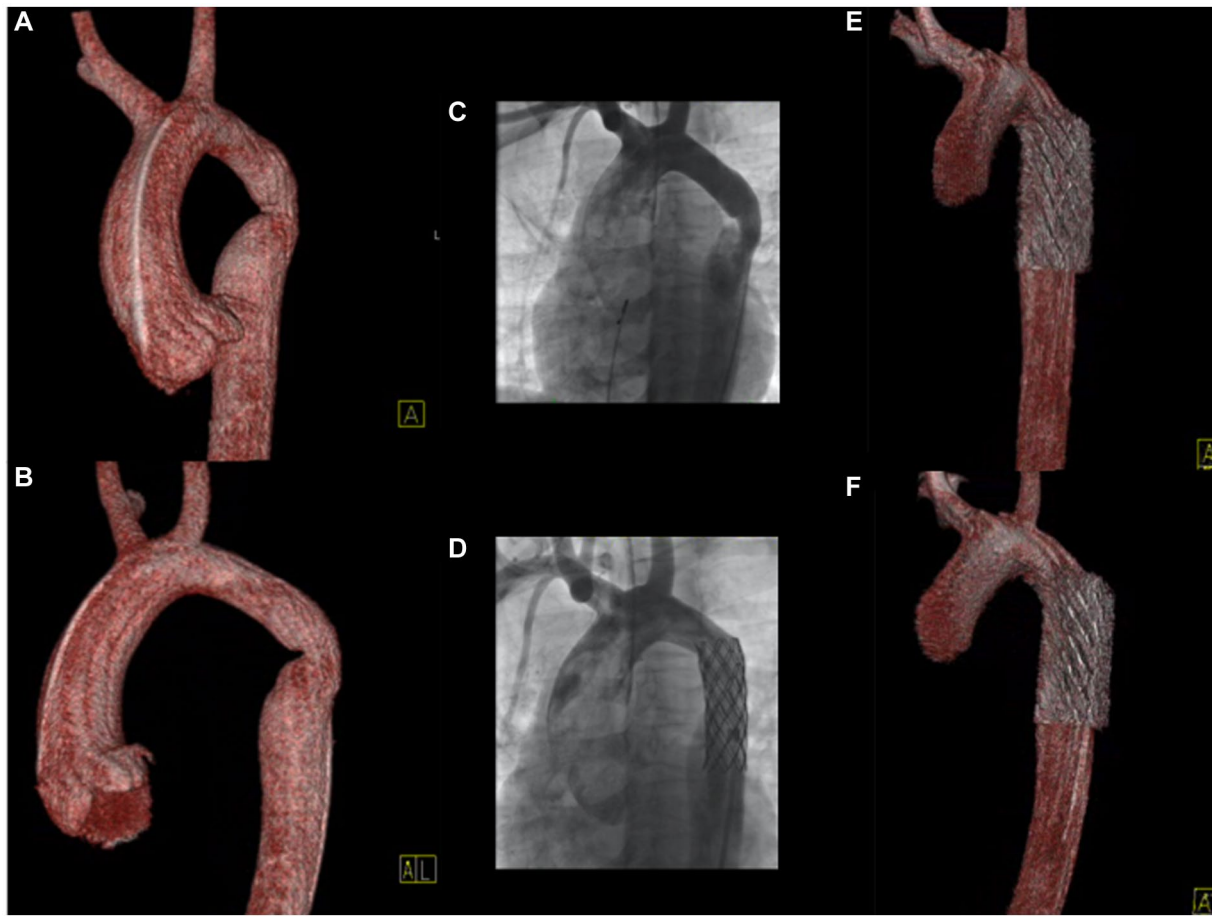


**FIGURE 5** (A, B) 3D rotational angiogram from a 15-year-old boy with re-coarctation after a subclavian flap repair, demonstrating the tortuosity of the stenosed arch, aiding selection of the optimal working view. (C) The corresponding 2D angiogram, and (D) implantation of a covered stent. (E, F) Post stent 3D-RA

## 6 | RADIATION EXPOSURE

Quantification of radiation burden is not straightforward with 3D-RA. One approach is using computed tomography dose index (CTDI), but this is problematic when applied to the wide cone beam in RA, as the extended irradiation field in the cranio-caudal direction exceeds the standard 100mm dose integration length, resulting in underestimation by 2%-5%.<sup>79,80</sup> Additionally, the anisotropic dose distribution, due to the course of the C-arm rotation with an angular range below 360°, is incongruent with the weightings of central and peripheral dose defined in CTDI.<sup>79,81</sup> Similarly, effective dose (ED) estimation based on dose area product (DAP) and conversion coefficients for single static projections are not applicable for RA.<sup>81,82</sup> To overcome these limitations, various dosimetry methodologies have been proposed, such as the use of large anthropomorphic phantoms equipped with thermoluminescent dosimeters, Monte Carlo-based computer simulation codes such as PCXMC, or adaptation of the CTDI integration length and a 600mm long phantom, as recommended by the International Commission on Radiation Units and Measurements (ICRU) in its Report 87.<sup>25,83-85</sup>

A few observations are notable from published studies utilizing 3D-RA in congenital cardiac catheterizations.<sup>5-9,41,42,44-47,49,50,58,69,81,84-87</sup> Phantom ED calculations result in significantly lower ED than real time calculations in children and should be interpreted with care.<sup>84,85</sup> ED approximations using Monte Carlo-based computer simulation codes correlate with DAP<sup>84,85</sup> but are significantly higher for smaller children when subgroup analysis was performed at the following cut offs: <30, <45, and <50 kg.,<sup>46,49,85,87</sup> supporting lower dose protocols for smaller children. When low dose protocols tailored to size are implemented, dose reduction is achievable without significant compromise to image quality.<sup>50,81,88,89</sup> The operator needs to work with the X-ray equipment vendor to establish low dose protocols for various subject weight categories. Increased BMI ( $\geq 30$  kg/m<sup>2</sup>) was highly predictive of poor image quality,<sup>90</sup> and in such patients 3D digital subtraction RA can be employed to improve image resolution.<sup>87</sup> The technique of soft tissue subtraction allows better visualization of vascular structures without superimposed bone and soft tissues, and the total procedure radiation is comparable to that of standard 3D-RA.<sup>87</sup>

While variability in both radiation dosimetry and exposure is evident, comparable or lower exposure rates to standard biplane



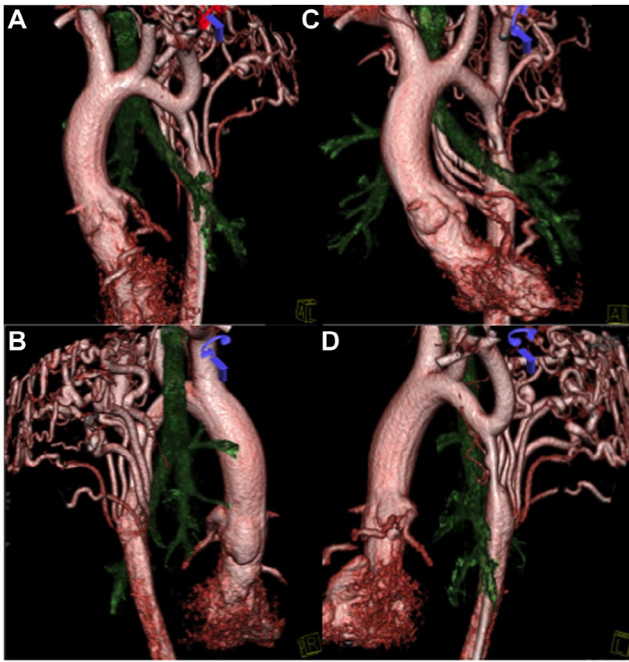


**FIGURE 6** 3D-RA of a 2-year-old boy referred for balloon angioplasty of an arch coarctation showing significant transverse arch hypoplasia and a long-segment isthmal coarctation with significant collateralization, and its relationship to the airways. This child was referred for surgical arch augmentation and coarctation repair

angiographic acquisitions were reported in all<sup>5,6,44,45,50,58,69,81,85</sup> but one study.<sup>49</sup> This study, however, reported significant radiation dose reduction after implementation of a dose-optimized protocol in collaboration with the manufacturer,<sup>49</sup> a finding echoed by other studies.<sup>5,42</sup> Additionally, a few studies have reported procedure-specific radiation doses that compare favorably to previously established pediatric benchmarks from large multicenter studies, namely PPVI and coarctation interventions.<sup>45,58,91,92</sup> The published median ED for the aforementioned procedures range from 0.16 to 1.8mSv,<sup>47,84,85,87</sup> which are significantly lower than the median exposure of 5.5 to 12mSv used in pediatric congenital cardiac MDCT angiography.<sup>40</sup>

## 6.1 | Dose optimization strategies

With increasing recognition of the lifetime risks associated with cumulative exposure to medical radiation, dose-reduction strategies are of importance, especially in this young and highly radiosensitive population.<sup>93,94</sup>

### 6.1.1 | Frame rate reduction

The total number of projections per rotation or frame rate provides a trade-off between image quality and the delivered dose. Several studies have reported significant dose reduction by applying frame rate reduction (to 30 frames/s or lower), while preserving image quality.<sup>45,58,84</sup>

### 6.1.2 | Acquisition technique (protocol) selection

Acquisition parameters are configurable in 3D-RA, including X-ray tube voltage (kV), tube current (mA), pulse width (ms), added filtration (material and thickness), and detector dose. Many of these parameters can be modified by the vendor to ensure sufficient image quality at the lowest achievable radiation dose. To balance optimal image quality and radiation dose, collaboration between the laboratory radiation physicist and vendor is vital to adjust the factory default protocol with testing on phantoms.<sup>25,49,85</sup> To this end, separation of dose protocols according to patient size and weight has important benefit, as alluded to earlier.

There are substantial differences in organ dose as a function of the projection angle, as the dose is modulated throughout the rotation. Three-dimensional RA typically uses automatic exposure control (AEC) systems, which modulate tube current based on active feedback from the detector. The AEC performance in various devices may be different in terms of modulation algorithms (eg, attenuation-based, sinusoidal-based, timing with automatic feedback), pre-programmed algorithms or a combination of these methods. Utilization of the AEC system with appropriate selection of the parameters can reduce radiation dose by 20%-40%, depending on the imaging task.<sup>25,85,95,96</sup>

### 6.1.3 | Inclusion of only the ROI in the image

Unnecessary body parts in the image have dose consequences and may also increase image artifacts significantly. Positioning the arms outside the irradiated area can reduce the level of artifacts, thus increasing the image quality without increasing unnecessary radiation dose.

### 6.1.4 | Anti-scatter grid removal

Anti-scatter grids improve the image contrast at the cost of increased patient radiation dose. In patients with small body habitus, a significant reduction in radiation dose is possible, without compromising image quality, by removal of the anti-scatter grid.<sup>97</sup>

### 6.1.5 | Radiation surveillance

With increasing use of 3D-RA in congenital cardiac catheterization, establishment of procedure-specific radiation exposure benchmarks and standardized dosimetry will help direct efforts in minimizing radiation doses.<sup>25,58</sup> Ultimately, the development and implementation of diagnostic reference levels to identify examinations above 75th percentile dose is an important dose optimization tool and has shown good results in many countries.<sup>25</sup>

## 7 | FUTURE PERSPECTIVES

A number of groups have applied MRI-based four-dimensional (4D) flow in congenital cardiac lesions, including quantification of ventricular



kinetic energy in patients with repaired tetralogy of Fallot as a novel imaging biomarker of ventricular dysfunction and evaluation of wall shear stress and pressure gradients across coarctation of the aorta to guide surgical and percutaneous interventions.<sup>98-101</sup> Efforts are now being made to bring dynamic multiphase 4D-RA to the cardiac catheterization laboratory. Beyond time resolved morphological data, 4D-RA holds promise for functional analysis such as ventricular volumetrics and 4D flows.<sup>102,103</sup> It utilizes retrospective ECG-gating, so that 3D reconstructions of multiple heart phases can be achieved. A key requirement for useful application is ensuring that a sufficient number of heart cycles are acquired during the scan. This can be achieved through a sufficiently high heart rate by cardiac pacing, but a non-physiologic contraction pattern limits this as a clinical tool. Alternatively, the acquisition time can be increased with an undesirable expense of higher radiation and contrast dose. Clinically feasible acquisition protocols currently pose a challenging reconstruction problem due to sparse angular sampling of the trajectory, with accompanying increase in noise and other artifacts.<sup>102</sup> Possible solutions include the use of a compressed sensing algorithm, based on algebraic reconstruction techniques with spatial and temporal total variation regularization. Recent work evaluating this algorithm showed that dynamic cardiac images can be effectively recovered from sparsely sampled data (as few as seven projections per heart phase). In addition, there was a high correlation of subsequent segmentation-based volumetry compared to less sparsely sampled data.<sup>25,102</sup> Other post-reconstruction filtering techniques such as inter-phase registration have also been used for noise and artifact reduction to improve the accuracy of the 4D image overlay.<sup>104</sup> Further work will be directed toward development of acquisition protocols with clinically acceptable radiation and contrast dose at physiological heart rate in sinus rhythm, and hardware and software reconstruction processes will be optimized to produce high fidelity dynamic images to enable clinically meaningful functional assessment.

Another area of research interest is the application of computational fluid dynamics (CFD) on 3D- or 4D-RA data. The benefits of CFD flow assessment in patients with single ventricular physiology and aortic coarctation for surgical- or catheter-based treatment planning and outcome prediction have been demonstrated, using MRI and CT.<sup>105-110</sup> Different to the measurement-based 4D flow, image-based CFD uses computer-based hemodynamic simulation to analyze fluid flow based on the laws of physics. Although MRI-based CFD in aortic coarctation has shown encouraging results in the prediction of pressure gradients compared to cardiac catheterization, the differing physiological status during MRI (awake) and catheterization (sedated or anesthetized) pose a limitation for direct comparison.<sup>110</sup> In contrast, 3D- or 4D-RA-based CFD represents a one-stop solution for real-time hemodynamic and anatomic assessment before and after intervention. Additionally, CFD allows virtual interventions and predictive modeling to optimize treatment, such as determining the optimal length, diameter, and location of stents.

Finally, several technical developments in 3D-RA and reconstruction software are expected to enable new features that will affect image quality and imparted radiation. An advanced AEC system to include variation in tube voltage, in addition to current modulation, is likely to improve radiation exposure control.<sup>25</sup> However, this makes

dose estimation very complex, mandating further research in this area. A shift to the iterative algorithms, as opposed to the analytical FDK approach, will enable high-resolution reconstruction from fewer projections with more robust noise and artifact suppression. These reconstruction methods also have the ability to incorporate prior knowledge of the anatomy, as well as radiation and scatter distribution, an advantageous feature when repetitive scanning of the same anatomical region is necessary, such as pre- and post-angiographic device deployment. Because changes in these successive 3D volumes are relatively minor, the number of input projections required for 3D reconstruction can be further reduced, hence decreasing overall radiation dose.<sup>25</sup> Another innovation in the pipeline is biplane rotational angiography, involving 90-degree rotation of each plane. The angiographic system incorporates two detectors, and a new imaging chain with an integrated 3D workstation to streamline data processing and 3D image reconstruction. (Siemens Medical personal communication).

## 8 | CONCLUSIONS

Three-dimensional RA has proven to be an excellent method for 3D evaluation of congenital cardiac lesions and image guided therapy in the catheterization laboratory, by improving visualization of complex structures and interactions, guiding interventions, and often decreasing radiation exposure. Considering the availability of other non-invasive 3D imaging modalities, the justification for using 3D-RA is linked intricately to its combined diagnostic and therapeutic efficacies in a one-stop shop environment. Further work is warranted in standardization of dosimetry and procedure specific radiation exposure, while preserving the expectation of high image quality and excellent clinical outcomes. Continual technological innovations and refinement of image processing techniques are paving the way for further evolution of 3D-RA to provide greater relevance in anatomical and functional assessment of congenital heart lesions as well as in predicting treatment outcomes.

## ACKNOWLEDGMENTS

The authors thank Nicholas Shkumat (Medical physicist for medical diagnostic imaging, The Hospital for Sick Children) for intellectual discussions and editorial input on the subject of radiation exposure in this manuscript.

## CONFLICT OF INTEREST

The authors declare that they have no conflicts of interest with the contents of the article.

## AUTHOR CONTRIBUTIONS

Sok-Leng Kang wrote the first draft of the article. Aimee Armstrong, Gregor Krings, and Lee Benson revised it critically for important intellectual content. All authors have read and approved the final manuscript.

## ORCID

Sok-Leng Kang  <https://orcid.org/0000-0003-1556-7395>

Lee Benson  <https://orcid.org/0000-0002-1407-1825>

## REFERENCES

1. Simpson J, Lopez L, Acar P, et al. Three-dimensional echocardiography in congenital heart disease: an expert consensus document from the European Association of Cardiovascular Imaging and the American Society of Echocardiography. *J Am Soc Echocardiogr*. 2017;30:1-27.
2. Puranik R, Muthurangu V, Celermajer DS, Taylor AM. Congenital heart disease and multi-modality imaging. *Heart Lung Circ*. 2010;19:133-144.
3. Samyn MM. A review of the complementary information available with cardiac magnetic resonance imaging and multi-slice computed tomography (CT) during the study of congenital heart disease. *Int J Cardiovasc Imaging*. 2004;20:569-578.
4. Crean A. Cardiovascular MR and CT in congenital heart disease. *Heart*. 2007;93:1637-1647.
5. Glatz AC, Zhu X, Gillespie MJ, Hanna BD, Rome JJ. Use of angiographic CT imaging in the cardiac catheterization laboratory for congenital heart disease. *JACC Cardiovasc Imaging*. 2010;3:1149-1157.
6. Kapins C, Barbosa F, Silva C, Lima V, Carvalho A. Use of rotational 3D (3D-RA) in congenital heart disease patients: experience with 53 cases. *Rev Bras Cardiol Invasiva*. 2010;18:199-203.
7. Glöckler M, Koch A, Greim V, et al. The value of flat-detector computed tomography during catheterisation of congenital heart disease. *Eur Radiol*. 2011;21:2511-2520.
8. Glockler M, Halbfabeta J, Koch A, Achenbach S, Dittrich S. Multimodality 3D-roadmap for cardiovascular interventions in congenital heart disease—a single-center, retrospective analysis of 78 cases. *Catheter Cardiovasc Interv*. 2013;82:436-442.
9. Aldoss O, Fonseca BM, Truong UT, et al. Diagnostic utility of three-dimensional rotational angiography in congenital cardiac catheterization. *Pediatr Cardiol*. 2016;37:1211-1221.
10. Fagan TE, Truong UT, Jone P-N, et al. Multimodality 3-dimensional image integration for congenital cardiac catheterization. *Methodist Debaquey Cardiovasc J*. 2014;10:68-76.
11. Campeau L, Saliel J. Rotational cineangiography. *Am J Roentgenol Radium Ther Nucl Med*. 1964;91:544-549.
12. Schad N, Brunner H. [Cineangiography of congenital heart defects with rotation of the patient] *Med Audio Vis*. 1966;5:59-64.
13. Cornelis G, Bellet A, van Eygen B, Roisin P, Libon E. Rotational multiple sequence roentgenography of intracranial aneurysms. *Acta Radiol Diagn*. 1972;13:74-76.
14. Thron A, Voigt K. Rotational cerebral angiography: procedure and value. *Am J Neuroradiol*. 1983;4:289-291.
15. Carsin M, Chabert E, Croci S, Romeas R, Scarabin JM. [The role of 3-dimensional reconstructions in the angiographic evaluation of cerebral vascular malformations: 3D morphometry] *J Neuroradiol*. 1997;24:137-140.
16. Anxionnat R, Bracard S, Macho J, et al. 3D angiography. Clinical interest. First applications in interventional neuroradiology. *J Neuroradiol*. 1998;25:251-262.
17. Irie K, Murayama Y, Saguchi T, et al. Dynact soft-tissue visualization using an angiographic C-arm system: initial clinical experience in the operating room. *Neurosurgery*. 2008;62:266-272; discussion 272.
18. Biasi L, Ali T, Thompson M. Intra-operative dynaCT in visceral-hybrid repair of an extensive thoracoabdominal aortic aneurysm. *Eur J Cardiothorac Surg*. 2008;34:1251-1252.
19. Kim H-C, Chung JW, Park JH, et al. Transcatheter arterial chemo-embolization for hepatocellular carcinoma: prospective assessment of the right inferior phrenic artery with C-arm CT. *J Vasc Interv Radiol*. 2009;20:888-895.
20. Murayama Y, Irie K, Saguchi T, et al. Robotic digital subtraction angiography systems within the hybrid operating room. *Neurosurgery*. 2011;68:1427-1433; discussion 1433.
21. Tommasini G, Camerini A, Gatti A, Derchi G, Bruzzone A, Vecchio C. Panoramic coronary angiography. *J Am Coll Cardiol*. 1998;31:871-877.
22. Raman SV, Morford R, Neff M, et al. Rotational X-ray coronary angiography. *Catheter Cardiovasc Interv*. 2004;63:201-207.
23. Orlov MV, Hoffmeister P, Chaudhry GM, et al. Three-dimensional rotational angiography of the left atrium and esophagus—A virtual computed tomography scan in the electrophysiology lab? *Heart Rhythm*. 2007;4:37-43.
24. Panzer J, Taeymans Y, De Wolf D. Three-dimensional rotational angiography of a patient with pulmonary atresia intact septum and coronary fistulas. *Pediatr Cardiol*. 2008;29:686-687.
25. Icrp R, Gupta R, et al. Radiological protection in cone beam computed tomography (CBCT). ICRP publication 129. *Ann ICRP*. 2015;44:9-127.
26. Pedra CA, Fleishman C, Pedra SF, Cheatham JP. New imaging modalities in the catheterization laboratory. *Curr Opin Cardiol*. 2011;26:86-93.
27. Berman D. Role of three-dimensional rotational angiography in imaging the pulmonary arteries. In: Butera G, Cheatham J, Pedra C, Schranz D, Tulzer G, eds. *Fetal and Hybrid Procedures in Congenital Heart Diseases*. Cham, Switzerland: Springer International Publishing; 2016:728-747.
28. Feldkamp L, Davis LC, Kress J. Practical cone-beam algorithm. *J Opt Soc Am*. 1984;6:612-619.
29. Schulze R, Heil U, Groß D, et al. Artefacts in CBCT: a review. *Dentomaxillofac Radiol*. 2011;40:265-273.
30. Sharma N, Ray AmitK, Shukla KK, et al. Automated medical image segmentation techniques. *J Med Phys*. 2010;35:3-14.
31. Schoenhagen P, Numburi U, Halliburton SS, et al. Three-dimensional imaging in the context of minimally invasive and transcatheter cardiovascular interventions using multi-detector computed tomography: from pre-operative planning to intra-operative guidance. *Eur Heart J*. 2010;31:2727-2740.
32. Aboulhosn J. Rotational angiography and 3D overlay in transcatheter congenital interventions. *Interv Cardiol*. 2013;5:405-410.
33. Krishnaswamy A, Tuzcu EM, Kapadia SR. Integration of MDCT and fluoroscopy using C-arm computed tomography to guide structural cardiac interventions in the cardiac catheterization laboratory. *Catheter Cardiovasc Interv*. 2015;85:139-147.
34. Krishnaswamy A, Tuzcu EM, Kapadia SR. Three-dimensional computed tomography in the cardiac catheterization laboratory. *Catheter Cardiovasc Interv*. 2011;77:860-865.
35. Goreczny S, Moszura T, Dryzek P, et al. Three-dimensional image fusion guidance of percutaneous pulmonary valve implantation to reduce radiation exposure and contrast dose: a comparison with traditional two-dimensional and three-dimensional rotational angiographic guidance. *Neth Heart J*. 2017;25:91-99.
36. Goreczny S, Dryzek P, Moszura T, Kuhne T, Berger F, Schubert S. 3D image fusion for live guidance of stent implantation in aortic coarctation – magnetic resonance imaging and computed tomography image overlay enhances interventional technique. *Adv Interv Cardiol*. 2017;13:269-272.
37. Goreczny S, Dryzek P, Morgan GJ, Lukaszewski M, Moll JA, Moszura T. Novel three-dimensional image fusion software to facilitate guidance of complex cardiac catheterization: 3D image fusion for interventions in CHD. *Pediatr Cardiol*. 2017;38:1133-1142.

38. Parimi M, Buelter J, Thanugundla V, et al. Feasibility and validity of printing 3d heart models from rotational angiography. *Pediatr Cardiol.* 2018;39:653–658.
39. Bai M, Liu B, Mu H, Liu X, Jiang Y. The comparison of radiation dose between C-arm flat-detector CT (DynaCT) and multi-slice CT (MSCT): a phantom study. *Eur J Radiol.* 2012;81:3577–3580.
40. Brody AS, Frush DP, Huda W, Brent RL; American Academy of Pediatrics Section on R. Radiation risk to children from computed tomography. *Pediatrics.* 2007;120:677–682.
41. Glöckler M, Koch A, Halbfäß J, et al. Assessment of cavopulmonary connections by advanced imaging: value of flat-detector computed tomography. *Cardiol Young.* 2013;23:18–26.
42. Berman DP, Khan DM, Gutierrez Y, Zahn EM. The use of three-dimensional rotational angiography to assess the pulmonary circulation following cavo-pulmonary connection in patients with single ventricle. *Catheter Cardiovasc Interv.* 2012;80:922–930.
43. Borik S, Volodina S, Chaturvedi R, Lee KJ, Benson LN. Three-dimensional rotational angiography in the assessment of vascular and airway compression in children after a cavopulmonary anastomosis. *Pediatr Cardiol.* 2015;36:1083–1089.
44. Stenger A, Dittrich S, Glockler M. Three-dimensional rotational angiography in the pediatric cath lab: optimizing aortic interventions. *Pediatr Cardiol.* 2016;37:528–536.
45. Starmans NL, Krings GJ, Molenschot MM, van der Stelt F, Breur JM. Three-dimensional rotational angiography in children with an aortic coarctation. *Neth Heart J.* 2016;24:666–674.
46. Pockett CR, Moore JW, El-Said HG. Three dimensional rotational angiography for assessment of coronary arteries during melody valve implantation: introducing a technique that may improve outcomes. *Neth Heart J.* 2017;25:82–90.
47. Truong UT, Fagan TE, Deterding R, Ing RJ, Fonseca BM. Use of rotational angiography in assessing relationship of the airway to vasculature during cardiac catheterization. *Catheter Cardiovasc Interv.* 2015;86:1068–1077.
48. Zahn E. The emerging use of 3-Dimensional rotational Angiography in congenital heart disease. *Congenital Cardiol Today.* 2011;9:1–13.
49. Manica JL, Borges MS, Medeiros RF, Fischer Ldos S, Broetto G, Rossi Filho RI. A comparison of radiation dose between standard and 3D angiography in congenital heart disease. *Arq Bras Cardiol.* 2014;103:131–137.
50. Thoenes C, Cesnjevar R, Dittrich S, Glockler M. Rotational angiography for 3D roadmapping of catheter interventions in congenital heart disease: comparison of a diagnostic and a low dose program. *Open J Radiol.* 2016;6:210–219.
51. Fagan T, Kay J, Carroll J, Neubauer A. 3-D guidance of complex pulmonary artery stent placement using reconstructed rotational angiography with live overlay. *Catheter Cardiovasc Interv.* 2012;79:414–421.
52. Hu Y, Xie L, Nunes JC, Bellanger JJ, Bedossa M, Toumoulin C. ECG gated tomographic reconstruction for 3-D rotational coronary angiography. *Conf Proc IEEE Eng Med Biol Soc.* 2010;2010:3614–3617.
53. Schafer D, Borgert J, Rasche V, Grass M. Motion-compensated and gated cone beam filtered back-projection for 3-D rotational X-ray angiography. *IEEE Trans Med Imaging.* 2006;25:898–906.
54. Unberath M, Aichert A, Achenbach S, Maier A. Consistency-based respiratory motion estimation in rotational angiography. *Med Phys.* 2017;44:e113–e124.
55. Müller K, Schwemmer C, Hornegger J, et al. Evaluation of interpolation methods for surface-based motion compensated tomographic reconstruction for cardiac angiographic C-arm data. *Med Phys.* 2013;40:031107.
56. Schultz CJ, Lauritsch G, Van Mieghem N, et al. Rotational angiography with motion compensation: first-in-man use for the 3D evaluation of transcatheter valve prostheses. *EuroIntervention.* 2015;11:442–449.
57. Poterucha JT, Foley TA, Taggart NW. Percutaneous pulmonary valve implantation in a native outflow tract: 3-dimensional DynaCT rotational angiographic reconstruction and 3-dimensional printed model. *JACC Cardiovasc Interv.* 2014;7:e151–e152.
58. Nguyen HH, Balzer DT, Murphy JJ, Nicolas R, Shahnavaz S. Radiation exposure by three-dimensional rotational angiography (3DRA) during trans-catheter melody pulmonary valve procedures (TMPV) in a pediatric cardiac catheterization laboratory. *Pediatr Cardiol.* 2016;37:1429–1435.
59. Guccione P, Milanesi O, Hijazi ZM, Pongiglione G. Transcatheter pulmonary valve implantation in native pulmonary outflow tract using the Edwards SAPIEN transcatheter heart valve. *Eur J Cardiothorac Surg.* 2012;41:1192–1194.
60. Bertels RA, Blom NA, Schaliij MJ. Edwards SAPIEN transcatheter heart valve in native pulmonary valve position. *Heart.* 2010;96:661.
61. Levi DS, Sinha S, Salem MM, Aboulhosn JA. Transcatheter native pulmonary valve and tricuspid valve replacement with the sapien XT: Initial experience and development of a new delivery platform. *Catheter Cardiovasc Interv.* 2016;88:434–443.
62. Thanopoulos BV, Giannakoulas G, Arampatzis CA. Percutaneous pulmonary valve implantation in the native right ventricular outflow tract. *Catheter Cardiovasc Interv.* 2012;79:427–429.
63. Chung R, Taylor AM. Imaging for preintervention planning: transcatheter pulmonary valve therapy. *Circ Cardiovasc Imaging.* 2014;7:182–189.
64. Malone L, Fonseca B, Fagan T, et al. Preprocedural risk assessment prior to PPVI with CMR and cardiac CT. *Pediatr Cardiol.* 2017;38:746–753.
65. Hill J, Bellotti C, Golden A. Three-dimensional rotational angiography during percutaneous device closure of Fontan fenestration. *World J Pediatr Congenit Heart Surg.* 2013;4:324–325.
66. Lapierre C, Dubois J, Rypens F, Raboisson MJ, Dery J. Tetralogy of fallot: preoperative assessment with MR and CT imaging. *Diagn Interv Imaging.* 2016;97:531–541.
67. Krings GJ, van der Stelt F, Molenschot MC, Breur JM. Oval stenting in left pulmonary artery stenosis: a novel double balloon technique to prevent airway compression in single ventricle. *EuroIntervention.* 2019. pii: EIJ-D-18-01079. doi: 10.4244/EIJ-D-18-01079
68. Goreczny S, Dryzek P, Moszura T, et al. [Rotational angiography in monitoring of covered CP stent implantation in patient with critical aortic coarctation and patent ductus arteriosus] *Kardiologia Pol.* 2012;70:505–507.
69. Goreczny S, Morgan GJ, Dryzek P, Moll JA, Moszura T. Initial experience with live three-dimensional image overlay for ductal stenting in hypoplastic left heart syndrome. *EuroIntervention.* 2016;12:1527–1533.
70. Rigatelli G, Zamboni A, Cardaioli P. Three-dimensional rotational digital angiography in a complicated case of patent ductus arteriosus transcatheter closure. *Catheter Cardiovasc Interv.* 2007;70:900–903.
71. Rigatelli G, Zamboni A, Cardaioli P, et al. Three-dimensional rotational digital angiography in catheter-based congenital heart disease interventions. *J Cardiovasc Med.* 2008;9:432.
72. Hudson PA, Klein AJ, Kim MS, et al. A novel dual-axis rotational coronary angiography evaluation of coronary artery disease—case presentation and review. *Clin Cardiol.* 2010;33:E16–E19.
73. Klein AJ, Garcia JA, Hudson PA, et al. Safety and efficacy of dual-axis rotational coronary angiography vs. standard coronary angiography. *Catheter Cardiovasc Interv.* 2011;77:820–827.
74. Maddux JT, Wink O, Messenger JC, et al. Randomized study of the safety and clinical utility of rotational angiography versus standard angiography in the diagnosis of coronary artery disease. *Catheter Cardiovasc Interv.* 2004;62:167–174.
75. Garcia JA, Agostoni P, Green NE, et al. Rotational vs. standard coronary angiography: an image content analysis. *Catheter Cardiovasc Interv.* 2009;73:753–761.

76. Akhtar M, Vakharia KT, Mishell J, et al. Randomized study of the safety and clinical utility of rotational vs. standard coronary angiography using a flat-panel detector. *Catheter Cardiovasc Interv.* 2005;66:43-49.
77. Rios R, Loomba RS, Foerster SR, Pelech AN, Gudauskas TM. Dual-axis rotational angiography is safe and feasible to detect coronary allograft vasculopathy in pediatric heart transplant patients: a single-center experience. *Pediatr Cardiol.* 2016;37:740-745.
78. Gudauskas TM, Pelech AN, Stendahl G, et al. Dual-axis rotational coronary angiography: a new technique for detecting graft coronary vasculopathy in pediatric heart transplant recipients. *Pediatr Cardiol.* 2013;34:560-565.
79. Kyriakou Y, Deak P, Langner O, Kalender WA. Concepts for dose determination in flat-detector CT. *Phys Med Biol.* 2008;53:3551-3566.
80. Sykes JR, Lindsay R, Iball G, Thwaites DI. Dosimetry of CBCT: methods, doses and clinical consequences. *J Phys: Conf Ser.* 2013;444:012017.
81. Reinke G, Dittrich S, Banckwitz R, et al. Three-dimensional rotational angiography in congenital heart disease: estimation of radiation exposure. *Open J Radiol.* 2013;3:124-129.
82. Wielandts JY, Smans K, Ector J, De Buck S, Heidebuchel H, Bosmans H. Effective dose analysis of three-dimensional rotational angiography during catheter ablation procedures. *Phys Med Biol.* 2010;55:563-579.
83. Pantos I, Patatoukas G, Katritsis DG, Efstathopoulos E. Patient radiation doses in interventional cardiology procedures. *Curr Cardiol Rev.* 2009;5:1-11.
84. Peters M, Krings G, Koster M, Molenschot M, Freund MW, Breur JM. Effective radiation dosage of three-dimensional rotational angiography in children. *Europace.* 2015;17:611-616.
85. Haddad L, Waller BR, Johnson J, et al. Radiation protocol for three-dimensional rotational angiography to limit procedural radiation exposure in the pediatric cardiac catheterization lab. *Congenit Heart Dis.* 2016;11:637-646.
86. Corredoira E, Vano E, Ubeda C, Gutierrez-Larraya F. Patient doses in paediatric interventional cardiology: impact of 3D rotational angiography. *J Radiol Prot.* 2015;35:179-195.
87. Surendran S, Waller BR, Elijovich L, et al. Use of 3-D digital subtraction rotational angiography during cardiac catheterization of infants and adults with congenital heart diseases. *Catheter Cardiovasc Interv.* 2017;90:618-625.
88. De Buck S, Alzand B, Wielandts J-Y, et al. Cardiac three-dimensional rotational angiography can be performed with low radiation dose while preserving image quality. *Europace.* 2013;15:1718-1724.
89. Minderhoud S, van der Stelt F, Molenschot M, Koster MS, Krings GJ, Breur J. Dramatic dose reduction in three-dimensional rotational angiography after implementation of a simple dose reduction protocol. *Pediatr Cardiol.* 2018;39:1635-1641.
90. Schultz CJ, van Mieghem NM, van der Boon RM, et al. Effect of body mass index on the image quality of rotational angiography without rapid pacing for planning of transcatheter aortic valve implantation: a comparison with multislice computed tomography. *Eur Heart J Cardiovasc Imaging.* 2014;15:133-141.
91. Ghelani SJ, Glatz AC, David S, et al. Radiation dose benchmarks during cardiac catheterization for congenital heart disease in the United States. *JACC Cardiovasc Interv.* 2014;7:1060-1069.
92. Kobayashi D, Meadows J, Forbes TJ, et al. Standardizing radiation dose reporting in the pediatric cardiac catheterization laboratory—a multicenter study by the CCISC (Congenital Cardiovascular Interventional Study Consortium). *Catheter Cardiovasc Interv.* 2014;84:785-793.
93. Beauséjour Ladouceur V, Lawler PR, Gurvitz M, et al. Exposure to low-dose ionizing radiation from cardiac procedures in patients with congenital heart disease: 15-year data from a population-based longitudinal cohort. *Circulation.* 2016;133:12-20.
94. Glatz AC, Purrington KS, Klinger A, et al. Cumulative exposure to medical radiation for children requiring surgery for congenital heart disease. *J Pediatr.* 2014;164:789-794.e10.
95. Soderberg M, Gunnarsson M. Automatic exposure control in computed tomography—an evaluation of systems from different manufacturers. *Acta Radiol.* 2010;51:625-634.
96. He W, Huda W, Magill D, Tavrides E, Yao H. Patient doses and projection angle in cone beam CT. *Med Phys.* 2010;37:2359-2368.
97. Justino H. The ALARA concept in pediatric cardiac catheterization: techniques and tactics for managing radiation dose. *Pediatr Radiol.* 2006;36(Suppl 2):146-153.
98. Goubergrits L, Mevert R, Yevtushenko P, et al. The impact of MRI-based inflow for the hemodynamic evaluation of aortic coarctation. *Ann Biomed Eng.* 2013;41:2575-2587.
99. Vasanaawala SS, Hanneman K, Alley MT, Hsiao A. Congenital heart disease assessment with 4D flow MRI. *J Magn Reson Imaging.* 2015;42:870-886.
100. Jeong D, Anagnostopoulos PV, Roldan-Alzate A, et al. Ventricular kinetic energy may provide a novel noninvasive way to assess ventricular performance in patients with repaired tetralogy of Fallot. *J Thorac Cardiovasc Surg.* 2015;149:1339-1347.
101. Stankovic Z, Allen BD, Garcia J, Jarvis KB, Markl M. 4D flow imaging with MRI. *Cardiovasc Diagn Ther.* 2014;4:173-192.
102. Taubmann O, Haase V, Lauritsch G, et al. Assessing cardiac function from total-variation-regularized 4D C-arm CT in the presence of angular undersampling. *Phys Med Biol.* 2017;62:2762-2777.
103. Müller K, Maier AK, Zheng Y, et al. Interventional heart wall motion analysis with cardiac C-arm CT systems. *Phys Med Biol.* 2014;59:2265-2284.
104. Wielandts JY, De Buck S, Ector J, Nuyens D, Maes F, Heidebuchel H. Left ventricular four-dimensional rotational angiography with low radiation dose through interphase registration. *Europace.* 2015;17:152-159.
105. Pennati G, Corsini C, Hsia TY, Migliavacca F. Modeling of Congenital Hearts Alliance I. Computational fluid dynamics models and congenital heart diseases. *Front Pediatr.* 2013;1:4.
106. DeCampi WM, Argueta-Morales IR, Divo E, Kassab AJ. Computational fluid dynamics in congenital heart disease. *Cardiol Young.* 2012;22:800-808.
107. Siallagan D, Loke Y-H, Olivieri L, et al. Virtual surgical planning, flow simulation, and 3-dimensional electrospinning of patient-specific grafts to optimize Fontan hemodynamics. *J Thorac Cardiovasc Surg.* 2017.
108. Roldan-Alzate A, Garcia-Rodriguez S, Anagnostopoulos PV, Srinivasan S, Wieben O, Francois CJ. Hemodynamic study of TCPC using in vivo and in vitro 4D Flow MRI and numerical simulation. *J Biomech.* 2015;48:1325-1330.
109. Ralovich K, Itu L, Vitanovski D, et al. Noninvasive hemodynamic assessment, treatment outcome prediction and follow-up of aortic coarctation from MR imaging. *Med Phys.* 2015;42:2143-2156.
110. Goubergrits L, Riesenkauff E, Yevtushenko P, et al. MRI-based computational fluid dynamics for diagnosis and treatment prediction: clinical validation study in patients with coarctation of aorta. *J Magn Reson Imaging.* 2015;41:909-916.

**How to cite this article:** Kang S-L, Armstrong A, Krings G, Benson L. Three-dimensional rotational angiography in congenital heart disease: Present status and evolving future. *Congenital Heart Disease.* 2019;14:1046-1057. <https://doi.org/10.1111/chd.12838>